Gauge-invariant measure of the magnon orbital angular momentum

Randy S. Fishman

Phys. Rev. B **107**, 214434 — Published 23 June 2023

DOI: 10.1103/PhysRevB.107.214434

A Gauge-Invariant Measure of the Magnon Orbital Angular Momentum

Randy S. Fishman[1,*]

[1] *Materials Science and Technology Division, Oak Ridge National Laboratory, Oak Ridge, Tennessee 37831, USA*

(Dated: June 5, 2023)

Unlike the Berry phase, the orbital angular momentum (OAM) of magnons with two-dimensional wavevector $\mathbf{k}$ in band n is not gauge invariant for arbitrary phase $\lambda_n(\mathbf{k})$ and so is not physically observable. However, by integrating the OAM over the orientation ϕ of wavevector $\mathbf{k}$, we construct a gauge-invariant function $F_n(k)$. Like $F_n(k)$, the average OAM for magnon band n in a circle of radius k is also gauge invariant and can be directly observed. We demonstrate these results for a ferromagnet on a honeycomb lattice with Dzyalloshinskii-Moriya interactions between next-nearest neighbor spins. With wavevectors $\mathbf{k}$ restricted to the first Brillouin zone, the angular averaged OAM $F_n(k)$ then has opposite signs for lower and upper bands $n = 1$ and 2 for all k.

I. INTRODUCTION

Magnons are quanta of spin excitations that can carry energy and information without incurring Joule heating. In some magnetic materials, magnons may travel over centimeter distances [1] before appreciable decay. Consequently, magnons have attracted a great deal of interest in the field of spintronics as replacements for electrons. While magnons have already exhibited a great many phenomenon of both scientific and technological interest such as the magnon thermal Hall [2–5], spin Seebeck [6, 7], and spin Nernst effects [8–10], the field of "magnonics" [11–13] has yet to reach full maturity.

Due to spin-orbit (SO) coupling, the spin Hall effect produces a spin current perpendicular to a charge current [14, 15]. Prior to its original observation by Onose *et al.* [16], the magnon Hall effect was predicted by Katsura *et al.* [17] using a Kubo formula that employed the Berry phase of a magnetic Hamiltonian. A magnon wavepacket with center of mass at position $\mathbf{r}_c$ obeys the semiclassical equation of motion [18]

$$\frac{d\mathbf{r}_c}{dt} = \frac{\partial\omega_n(\mathbf{k})}{\partial\mathbf{k}} - \frac{d\mathbf{k}}{dt}\times\mathbf{\Omega}_n(\mathbf{k}), \tag{1}$$

where $\omega_n(\mathbf{k})$ is the magnon frequency, $\mathbf{\Omega}_n(\mathbf{k})$ is the Berry phase for magnon band n and wavevector $\mathbf{k}$, and times is the cross product. This relation predicts the bending of the magnon wavepacket in the presence of Dzyalloshinskii-Moriya (DM) interactions created by SO coupling, i.e. the magnon Hall effect. Like DM interactions, dipole interactions can also produce a nonzero Berry phase in ferromagnets (FMs) [19]. The effects of the Berry phase induced by geometry on FMs in wires, ribbons, and spheres can be traced back to anisotropy and DM interaction energies [13]. For a FM in the absence of DM or dipole interactions, both the Berry phase and the magnon Hall effect vanish.

Like Ref. [17], most subsequent work on magnon dynamics borrowed heavily from the semiclassical theory of electronic band structure, with the Berry phase taking a central role [18]. Due to its roots in electronic band structure, the magnetic Berry phase is usually expressed in terms of Bloch functions $|u_n(\mathbf{k})\rangle$ as

$$\mathbf{\Omega}_n(\mathbf{k}) = \frac{i}{2\pi}\left\{\frac{\partial}{\partial\mathbf{k}}\times\langle u_n(\mathbf{k})|\frac{\partial}{\partial\mathbf{k}}|u_n(\mathbf{k})\rangle\right\}. \tag{2}$$

Earlier work on the Berry phase also specialized to FMs, so that the kinetic energy of a magnon can be written as $-(\hbar k)^2/2m^*$, in analogy with the electron kinetic energy, where m^* is the effective mass of the magnon. Parameterized in terms of m^*, results for the magnon thermal Hall conductivity and other transport properties are valid only at low energies and temperatures, where the dispersion of the FM magnon frequency $\omega_n(\mathbf{k})$ is quadratic.

Just as spin angular momentum underlays the magnetic interactions between moments, orbital angular momentum (OAM) underlays the Berry phase. From a purely formal perspective, Matusmoto and Murakami [20, 21] described the OAM as the "self rotation" of the magnon wavepacket. But from a physical point of view, the OAM of magnons has taken a decidedly secondary role to the Berry phase in earlier work.

Considering the importance of OAM in other fields such as optics [22–25] and electronic "orbitronics" [26–28], it is indeed surprising that more effort has not been made to understand the effects of OAM in thin film magnets. We expect that the OAM of magnons will play important roles in information storage, communications technology, and in the coupling between magnons and other particles that can carry OAM, like electrons [29], phonons [30, 31], and photons [32]. In particular, the interaction between the spin and OAM of magnons might be utilized to control the flow and lifetime of magnetic excitations.

* fishmanrs@ornl.gov

In the course of developing a quantum treatment for the magnon OAM, recent work [33, 34] provided four examples of collinear magnets where OAM appears when the exchange interactions create a non-Bravais lattice that violates inversion symmetry and channels the magnon motion in nontrivial ways. Two FMs and two antiferromagnets (AFs) were studied on zig-zag square lattices and honeycomb lattices.

Nevertheless, Refs. [33] and [34] side-stepped the important issue of gauge invariance [35]. While the Berry phase is invariant under the gauge transformation

$$|u_n(\mathbf{k})\rangle \to |u_n(\mathbf{k})\rangle\, e^{-i\lambda_n(\mathbf{k})} \tag{3}$$

for an arbitrary phase $\lambda_n(\mathbf{k})$, the OAM is *not* gauge invariant. Quantities that depend on gauge are not considered to be physically observable [18]. The absence of gauge invariance has stymied previous investigators and stalled earlier studies of the OAM. In this paper, we show that a gauge-invariant, physically measurable function $F_n(k)$ can be obtained by integrating the OAM over the orientation ϕ of the wavevector $\mathbf{k} = (k, \phi)$.

This paper is divided into five sections. In Section II, we review some of the formal development originally presented in Ref. [33], now extended by including further quantum effects and simplified for collinear magnets. Section III contains a derivation of the gauge invariant function $F_n(k)$. Section IV applies that function to the four case studies of Ref. [33]. The function $F_n(k)$ is nonzero only for a FM honeycomb lattice in the presence of DM interactions. Section V explains how to translate expressions between the semiclassical and quantum languages. A discussion is contained in Section VI.

II. QUANTUM FORMALISM

As discussed in Ref. [34], the classical equations of motion [36, 37] for the dynamical magnetization $\boldsymbol{\mu}_i = 2\mu_{\rm B}\,\delta\mathbf{S}_i$ of a collinear magnet at site i produce the linear momentum $\mathbf{p}_i$ [38]:

$$p_{i\alpha} = \frac{1}{4\mu_{\rm B} M_0}(\boldsymbol{\mu}_i \times \mathbf{n}_i)\cdot\frac{\partial \boldsymbol{\mu}_i}{\partial x_\alpha}, \tag{4}$$

where $M_0 = 2\mu_{\rm B} S$ is the static magnetization for a spin $\mathbf{S}_i$ pointing along $\mathbf{n}_i = \pm\mathbf{z}$. Using the $1/S$ quantization conditions $\overline{\mu}_i{}^+ = \mu_{ix} n_{iz} + i\mu_{iy} = 2\mu_{\rm B}\sqrt{2S\hbar}\,a_i$ and $\overline{\mu}_i{}^- = \mu_{ix} n_{iz} - i\mu_{iy} = 2\mu_{\rm B}\sqrt{2S\hbar}\,a_i^\dagger$ for the dynamical magnetization in terms of the local Boson operators a_i and $a_i^\dagger$ satisfying the momentum-space commutation relations $[a_{\mathbf{k}}^{(r)}, a_{\mathbf{k}'}^{(s)\dagger}] = \delta_{rs}\delta_{\mathbf{k},\mathbf{k}'}$ and $[a_{\mathbf{k}}^{(r)}, a_{\mathbf{k}'}^{(s)}] = 0$, the quantized linear and OAM are given by

$$\mathbf{p} = -\frac{\hbar}{2}\sum_{r=1}^{M}{\sum_{\mathbf{k}}}'\mathbf{k}\Big\{a_{\mathbf{k}}^{(r)\dagger}a_{\mathbf{k}}^{(r)} + a_{\mathbf{k}}^{(r)}a_{\mathbf{k}}^{(r)\dagger}\Big\}, \tag{5}$$

$$\begin{aligned}\mathcal{L}_z &= \sum_i (\mathbf{r}_i \times \mathbf{p}_i)\cdot\mathbf{z} \\ &= \frac{\hbar}{2}\sum_{r=1}^{M}{\sum_{\mathbf{k}}}'\Big\{a_{\mathbf{k}}^{(r)}\,\hat{l}_{z\mathbf{k}}\,a_{\mathbf{k}}^{(r)\dagger} - a_{\mathbf{k}}^{(r)\dagger}\,\hat{l}_{z\mathbf{k}}\,a_{\mathbf{k}}^{(r)}\Big\},\end{aligned} \tag{6}$$

where r and s refer to the M sites in the magnetic unit cell and

$$\hat{l}_{z\mathbf{k}} = -i\bigg(k_x\frac{\partial}{\partial k_y} - k_y\frac{\partial}{\partial k_x}\bigg) \tag{7}$$

is the OAM operator. The prime restricts the sum over wavevectors $\mathbf{k}$ to the first BZ of the magnetic unit cell. The first relation specifies how the linear momentum $\mathbf{p}$, which can take any value inside or outside the first BZ, is expressed in terms of wavevectors $\mathbf{k}$ solely within the first BZ.

In terms of the $a_{\mathbf{k}}^{(r)}$ and $a_{\mathbf{k}}^{(r)\dagger}$ operators, the second-order Hamiltonian H_2 can be written as

$$H_2 = {\sum_{\mathbf{k}}}'\mathbf{v}_{\mathbf{k}}^\dagger\cdot\underline{L}(\mathbf{k})\cdot\mathbf{v}_{\mathbf{k}}, \tag{8}$$

where the vector operators

$$\mathbf{v}_{\mathbf{k}} = (a_{\mathbf{k}}^{(1)}, a_{\mathbf{k}}^{(2)}\ldots a_{\mathbf{k}}^{(M)}, a_{-\mathbf{k}}^{(1)\dagger}, a_{-\mathbf{k}}^{(2)\dagger}\ldots a_{-\mathbf{k}}^{(M)\dagger}) \tag{9}$$

satisfy $[\mathbf{v}_{\mathbf{k}}, \mathbf{v}_{\mathbf{k}'}^\dagger] = \underline{N}\,\delta_{\mathbf{k},\mathbf{k}'}$ with

$$\underline{N} = \begin{pmatrix} \underline{I} & 0 \\ 0 & -\underline{I}\end{pmatrix} \tag{10}$$

and $\underline{I}$ is the M-dimensional identity matrix.

We then transform to the interacting vector operators

$$\mathbf{w}_{\mathbf{k}} = (b_{\mathbf{k}}^{(1)}, b_{\mathbf{k}}^{(2)}\ldots b_{\mathbf{k}}^{(M)}, b_{-\mathbf{k}}^{(1)\dagger}, b_{-\mathbf{k}}^{(2)\dagger}\ldots b_{-\mathbf{k}}^{(M)\dagger}), \tag{11}$$

which satisfy $[\mathbf{w}_{\mathbf{k}}, \mathbf{w}_{\mathbf{k}'}^\dagger] = \underline{N}\,\delta_{\mathbf{k},\mathbf{k}'}$. The relation between $\mathbf{v}_{\mathbf{k}}$ and $\mathbf{w}_{\mathbf{k}}$ is given by $\mathbf{v}_{\mathbf{k}} = \underline{X}^{-1}(\mathbf{k})\cdot\mathbf{w}_{\mathbf{k}}$, which may be expanded as

$$\begin{aligned} a_{\mathbf{k}}^{(r)} &= \sum_n\Big\{X^{-1}(\mathbf{k})_{rn}\,b_{\mathbf{k}}^{(n)} + X^{-1}(\mathbf{k})_{r,n+M}\,b_{-\mathbf{k}}^{(n)\dagger}\Big\}, \\ a_{-\mathbf{k}}^{(r)\dagger} &= \sum_n\Big\{X^{-1}(\mathbf{k})_{r+M,n}\,b_{\mathbf{k}}^{(n)} + X^{-1}(\mathbf{k})_{r+M,n+M}\,b_{-\mathbf{k}}^{(n)\dagger}\Big\}.\end{aligned} \tag{12}$$

The matrix $\underline{X}^{-1}(\mathbf{k})$ obeys the eigenvalue equation [39]

$$\underline{\Lambda}(\mathbf{k})\cdot\underline{X}^{-1}(\mathbf{k}) = \epsilon_n(\mathbf{k})\,\underline{X}^{-1}(\mathbf{k}), \tag{13}$$

where $\underline{\Lambda}(\mathbf{k}) = \underline{N}\cdot\underline{L}(\mathbf{k})$ and $\epsilon_n(\mathbf{k}) = \hbar\omega_n(\mathbf{k})/2$ ($n = 0,\ldots,M$) or $-\hbar\omega_n(-\mathbf{k})/2$ ($n = M+1,\ldots,2M$). This expression is the quantum analogue of the semiclassical relation

$$H_2|u_n(\mathbf{k})\rangle = \hbar\omega_n(\mathbf{k})|u_n(\mathbf{k})\rangle. \tag{14}$$

Hence, $X^{-1}(\mathbf{k})_{rn}$ can be considered the nth eigenfunction of the $2M\times 2M$ magnon energy matrix $\underline{\Lambda}(\mathbf{k})$.

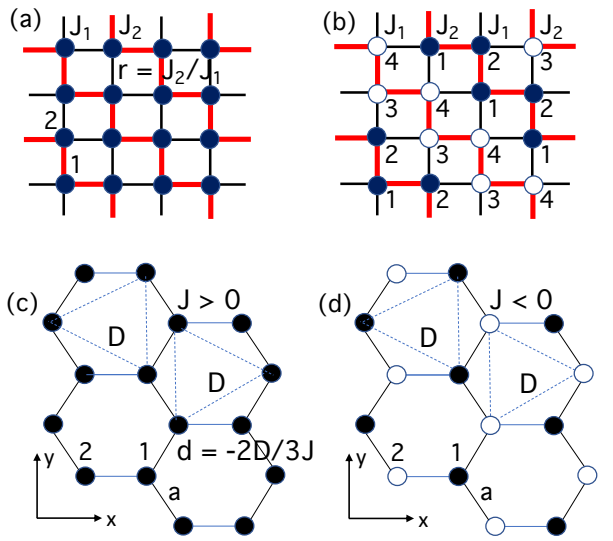

FIG. 1. Four case studies: (a) a zig-zag lattice with FM interactions $J_1 > 0$, $J_2 > 0$, and ratio $r = J_2/J_1$, (b) a zig-zag lattice with AF interaction $J_1 < 0$ and FM interaction $J_2 > 0$, (c) a honeycomb lattice with FM interaction $J > 0$ and DM interaction D between next-nearest neighbors with $d = -2D/3J$, and (d) a honeycomb lattice with AF interaction $J < 0$ and DM interaction D. In all cases, up spins are solid circles and down spins are empty circles.

In terms of the interacting Boson operators, we find

$$\mathbf{p} = -\frac{\hbar}{2}\sum_{n,\mathbf{k}}{}'\mathbf{k}\Big\{2b_{\mathbf{k}}^{(n)\dagger}b_{\mathbf{k}}^{(n)}+1\Big\}, \tag{15}$$

$$\mathcal{L}_z = \sum_{n,\mathbf{k}}{}'O_n(\mathbf{k})\Big\{2b_{\mathbf{k}}^{(n)\dagger}b_{\mathbf{k}}^{(n)}+1\Big\} + (\mathbf{r}_c\times\mathbf{p}_c)\cdot\mathbf{z}, \tag{16}$$

where

$$O_n(\mathbf{k}) = \frac{\hbar}{2}\sum_{r=1}^{M}\Big\{X^{-1}(\mathbf{k})_{rn}\,\hat{l}_{z\mathbf{k}}\,X^{-1}(\mathbf{k})^*_{rn} - X^{-1}(\mathbf{k})_{r+M,n}\,\hat{l}_{z\mathbf{k}}\,X^{-1}(\mathbf{k})^*_{r+M,n}\Big\}. \tag{17}$$

The last contribution $(\mathbf{r}_c\times\mathbf{p}_c)$ to $\mathcal{L}_z$ is the OAM of the center-of-mass of the magnon wavepacket, as defined by Chang and Niu [40].

Because the factor $2b_{\mathbf{k}}^{(n)\dagger}b_{\mathbf{k}}^{(n)}$ was treated incorrectly, Ref. [33] undercounted the OAM $\mathcal{L}_z$ for mode n by a factor of three [41]. Of course, $2\langle b_{\mathbf{k}}^{(n)\dagger}b_{\mathbf{k}}^{(n)}\rangle = 2$ for a single magnon with wavevector $\mathbf{k}$ in state n. For collinear spin states on a non-centrosymmetric lattice *without* DM interactions, time-reversal symmetry requires [26] $\underline{X}^{-1}(-\mathbf{k}) = \underline{X}^{-1}(\mathbf{k})^*$ so that $O_n(\mathbf{k}) = -O_n(-\mathbf{k})$ is an odd function of $\mathbf{k}$. It follows that the OAM for a given magnon band n would vanish when integrated over a ring of radius k within the two-dimensional BZ.

Using the semiclassical notation, the OAM can be written as

$$O_n(\mathbf{k}) = -\frac{i\hbar}{2}\Big\{\mathbf{k}\times\langle u_n(\mathbf{k})|\frac{\partial}{\partial\mathbf{k}}|u_n(\mathbf{k})\rangle\Big\}\cdot\mathbf{z}. \tag{18}$$

On the other hand, the Berry phase $\mathbf{\Omega}_n(\mathbf{k})$ can be written in terms of the quantum eigenfunctions $\underline{X}^{-1}(\mathbf{k})$ as

$$\mathbf{\Omega}_n(\mathbf{k}) = \frac{i}{2\pi}\sum_{r=1}^{M}\Big\{\frac{\partial X^{-1}(\mathbf{k})^*_{rn}}{\partial\mathbf{k}}\times\frac{\partial X^{-1}(\mathbf{k})_{rn}}{\partial\mathbf{k}} - \frac{\partial X^{-1}(\mathbf{k})^*_{r+M,n}}{\partial\mathbf{k}}\times\frac{\partial X^{-1}(\mathbf{k})_{r+M,n}}{\partial\mathbf{k}}\Big\}. \tag{19}$$

A guide to translating expressions between the semiclassical and quantum languages is provided in Section V.

III. GAUGE INVARIANCE

In the semiclassical language, each Bloch function $|u_n(\mathbf{k})\rangle$ can be multiplied by an arbitrary phase factor $\exp(-i\lambda_n(\mathbf{k}))$ as in Eq. (3). In the quantum language, each eigenfunction $X^{-1}(\mathbf{k})_{rn}$ can also be multiplied by an arbitrary phase factor so that

$$X^{-1}(\mathbf{k})_{rn} \to X^{-1}(\mathbf{k})_{rn}\,e^{-i\lambda_n(\mathbf{k})}, \tag{20}$$

where $\lambda_n(\mathbf{k})$ may depend on $\mathbf{k}$ and band index n but not on site r. Under a gauge transformation,

$$O_n(\mathbf{k}) \to O_n(\mathbf{k}) + \frac{\hbar}{2}\left(k_x\frac{\partial}{\partial k_y} - k_y\frac{\partial}{\partial k_x}\right)\lambda_n(\mathbf{k}), \tag{21}$$

$$\mathbf{\Omega}_n(\mathbf{k}) \to \mathbf{\Omega}_n(\mathbf{k}), \tag{22}$$

both of which use the normalization condition $\underline{X}^{-1}(\mathbf{k})\cdot\underline{N}\cdot\underline{X}^{-1\,\dagger}(\mathbf{k}) = \underline{N}$ (equivalent to $\langle u_n(\mathbf{k})|u_n(\mathbf{k})\rangle = 1$), or

$$\sum_{r=1}^{M}\Big\{|X^{-1}(\mathbf{k})_{rn}|^2 - |X^{-1}(\mathbf{k})_{r+M,n}|^2\Big\} = 1. \tag{23}$$

Whereas the Berry phase is invariant for any phase factor $\lambda_n(\mathbf{k})$, Eq. (21) indicates that the OAM is not.

After decomposing $\mathbf{k} = (k,\phi)$ in terms of its magnitude k and orientation ϕ, we find that

$$\left(k_x\frac{\partial}{\partial k_y} - k_y\frac{\partial}{\partial k_x}\right)\lambda_n(\mathbf{k}) = \frac{\partial}{\partial\phi}\lambda_n(k,\phi). \tag{24}$$

Due to the ϕ dependence of the phase $\lambda_n(\mathbf{k}) = \lambda_n(k,\phi)$, $O_n(\mathbf{k})$ is *not* gauge invariant. In order to obtain an observable measure of the OAM, we construct the function

$$F_n(k) = \int_0^{2\pi}\frac{d\phi}{2\pi}\,O_n(\mathbf{k}). \tag{25}$$

Under a gauge transformation,

$$\begin{aligned} F_n(k) &\rightarrow F_n(k) + \frac{\hbar}{2}\int_0^{2\pi}\frac{d\phi}{2\pi}\frac{\partial}{\partial\phi}\lambda_n(k,\phi) \\ &= F_n(k) + \frac{\hbar}{2}\Big\{\lambda_n(k,2\pi) - \lambda_n(k,0)\Big\} \\ &= F_n(k), \end{aligned} \tag{26}$$

which assumes only that $\lambda_n(\mathbf{k})$ is a single-valued function of the wavevector $\mathbf{k}$ [42]. Hence, $F_n(k)$ is a gauge-invariant function. Of course, $F_n(k)$ is nonzero only for a band n with a net OAM when integrated over a ring for all angles ϕ with a fixed k.

To better understand the results for $O_n(\mathbf{k})$, we can also evaluate the OAM averaged over a circle of radius k:

$$\begin{aligned} O_{n,\mathrm{av}}(k) &= \frac{2}{k^2}\int_0^k dq\, qF_n(q) \\ &= \frac{1}{\pi k^2}\int d\mathbf{q}\, O_n(\mathbf{q})\, H(k-q), \end{aligned} \tag{27}$$

where the Heaviside function $H(x)$ is defined so that $H(x) = 1$ for $x > 0$ and 0 otherwise. Like $F_n(k)$, $O_{n,\mathrm{av}}(k)$ is also gauge invariant.

IV. CASE STUDIES

Now consider the four examples sketched in Fig. 1 and discussed in Ref. [33]. Since DM interactions are absent for the FM and AF zig-zag lattices in Figs. 1(a) and (b), $O_n(\mathbf{k}) = -O_n(-\mathbf{k})$ is odd in $\mathbf{k}$. This immediately implies that $F_n(k) = 0$. For the AF honeycomb lattice in Fig. 1(d), DM interactions shift the magnon frequencies but do not affect the magnon energy matrix $\underline{\Lambda}(\mathbf{k}) = \underline{N}\cdot\underline{L}(\mathbf{k})$ in any non-trivial way. So once again $O_n(\mathbf{k}) = -O_n(-\mathbf{k})$ and $F_n(k) = 0$.

The only case that satisfies the condition $F_n(k) \neq 0$ is the FM honeycomb with $d = -2D/3J > 0$ shown in Fig. 1(c), where $J > 0$ is the nearest-neighbor exchange interaction and $D < 0$ is the next-nearest neighbor DM interaction, which breaks time-reversal symmetry. Strong easy-axis anisotropy $-K\sum_i {S_{iz}}^2$ prevents the spins from tilting away from the z axis. The 4×4 matrix $\underline{L}(\mathbf{k})$ defined by Eq. (8) can then be written

$$\underline{L}(\mathbf{k}) = \frac{3JS}{2}\begin{pmatrix} 1-G_{\mathbf{k}} & -\Gamma_{\mathbf{k}}^* & 0 & 0 \\ -\Gamma_{\mathbf{k}} & 1+G_{\mathbf{k}} & 0 & 0 \\ 0 & 0 & 1+G_{\mathbf{k}} & -\Gamma_{\mathbf{k}}^* \\ 0 & 0 & -\Gamma_{\mathbf{k}} & 1-G_{\mathbf{k}} \end{pmatrix}, \tag{28}$$

where $G_{\mathbf{k}} = d\,\Theta_{\mathbf{k}}$,

$$\Theta_{\mathbf{k}} = 4\cos(3k_xa/2)\sin(\sqrt{3}k_ya/2) - 2\sin(\sqrt{3}k_ya), \tag{29}$$

$$\Gamma_{\mathbf{k}} = \frac{1}{3}\Big\{e^{ik_xa} + 2e^{-ik_xa}\cos(\sqrt{3}k_ya/2)\Big\}. \tag{30}$$

The magnon mode energies are given by

$$\hbar\omega_1(\mathbf{k}) = 3JS(1+\kappa-\eta_{\mathbf{k}}), \tag{31}$$

$$\hbar\omega_2(\mathbf{k}) = 3JS(1+\kappa+\eta_{\mathbf{k}}), \tag{32}$$

with $\eta_{\mathbf{k}} = \sqrt{|\Gamma_{\mathbf{k}}|^2 + G_{\mathbf{k}}^2}$. Because the anisotropy $\kappa = 2K/3|J|$ merely shifts the magnon energies $\hbar\omega_n(\mathbf{k})$ but does not affect the OAM, its contribution to $\underline{L}(\mathbf{k})$ is omitted.

After some manipulations, we find

$$X^{-1}(\mathbf{k})_{11} = -\frac{1}{2c_1(\mathbf{k})\eta_{\mathbf{k}}}, \tag{33}$$

$$X^{-1}(\mathbf{k})_{12} = \frac{1}{2c_2(\mathbf{k})\eta_{\mathbf{k}}}, \tag{34}$$

$$X^{-1}(\mathbf{k})_{21} = \frac{\eta_{\mathbf{k}}+G_{\mathbf{k}}}{2c_1(\mathbf{k})\Gamma_{\mathbf{k}}^*\,\eta_{\mathbf{k}}}, \tag{35}$$

$$X^{-1}(\mathbf{k})_{22} = \frac{\eta_{\mathbf{k}}-G_{\mathbf{k}}}{2c_2(\mathbf{k})\Gamma_{\mathbf{k}}^*\,\eta_{\mathbf{k}}}, \tag{36}$$

while the 31, 32, 41, and 42 matrix elements of $\underline{X}^{-1}(\mathbf{k})$ vanish. The normalization condition $\underline{X}^{-1}(\mathbf{k})\cdot\underline{N}\cdot\underline{X}^{-1\,\dagger}(\mathbf{k}) = \underline{N}$ gives

$$c_1(\mathbf{k}) = \frac{e^{i\lambda_1(\mathbf{k})}}{\sqrt{2\eta_{\mathbf{k}}(\eta_{\mathbf{k}}-G_{\mathbf{k}})}}, \tag{37}$$

$$c_2(\mathbf{k}) = \frac{e^{i\lambda_2(\mathbf{k})}}{\sqrt{2\eta_{\mathbf{k}}(\eta_{\mathbf{k}}+G_{\mathbf{k}})}}. \tag{38}$$

Here, $\lambda_n(\mathbf{k})$ are arbitrary phases because the normalization conditions only determine the amplitudes $|c_n(\mathbf{k})|$. Since Eq. (13) is a linear eigenvalue equation, the column vectors $X_{rn}^{-1}(\mathbf{k})$ for modes $n = 1$ and 2 are only determined up to overall arbitrary phase factors $\exp(-i\lambda_n(\mathbf{k}))$.

Regardless of those phase factors, the Berry phase along $\mathbf{z}$ is given by

$$\Omega_{1z}(\mathbf{k}) = -i\frac{d}{4\pi}\frac{\Gamma_{\mathbf{k}}^*}{|\Gamma_{\mathbf{k}}|}\left\{\frac{\partial\Theta_{\mathbf{k}}/\eta_{\mathbf{k}}}{\partial\mathbf{k}}\times\frac{\partial\Gamma_{\mathbf{k}}/|\Gamma_{\mathbf{k}}|}{\partial\mathbf{k}}\right\}\cdot\mathbf{z}, \tag{39}$$

which is plotted in Fig. 2 for four different values of d. As the above expression makes clear, the Berry phase vanishes for $d = 0$. Notice that the Berry phase is six-fold symmetric and always positive for mode 1. The peaks of the Berry phase rotate by 30^o when d exceeds about 0.06. At that value for d, the maximum amplitude of the Berry phase reaches a minimum. For mode 2, $\Omega_{2z}(\mathbf{k}) = -\Omega_{1z}(\mathbf{k}) < 0$.

Since the DM interactions break time-reversal symmetry, $O_n(\mathbf{k})$ contains both even and odd terms with respect to $\mathbf{k}$ due to the $G_{\mathbf{k}} = -G_{-\mathbf{k}} \sim d$ functions in $\underline{X}^{-1}(\mathbf{k})$. Assuming that $c_1(\mathbf{k})$ and $c_2(\mathbf{k})$ are both real or

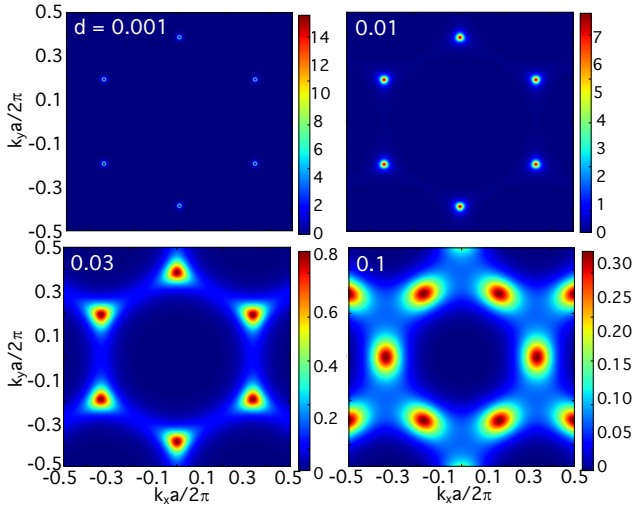

FIG. 2. Berry phase $\Omega_{1z}(\mathbf{k})/\hbar$ for a honeycomb lattice with FM exchange $J > 0$ between neighboring up spins and DM interaction D between next-neighbor as shown in Fig. 1(c) for values of $d = -2D/3J$ between 0.001 and 0.1, for band 1.

that $\lambda_n(\mathbf{k}) = 0$, the OAM for the lower and upper bands are given by

$$O_1(\mathbf{k}) = \frac{\hbar}{4}\left\{1 + \frac{d\,\Theta_{\mathbf{k}}}{\eta_{\mathbf{k}}}\right\}\frac{\Gamma_{\mathbf{k}}}{|\Gamma_{\mathbf{k}}|}\,\hat{l}_{z\mathbf{k}}\,\frac{\Gamma^*_{\mathbf{k}}}{|\Gamma_{\mathbf{k}}|}, \tag{40}$$

$$O_2(\mathbf{k}) = \frac{\hbar}{4}\left\{1 - \frac{d\,\Theta_{\mathbf{k}}}{\eta_{\mathbf{k}}}\right\}\frac{\Gamma_{\mathbf{k}}}{|\Gamma_{\mathbf{k}}|}\,\hat{l}_{z\mathbf{k}}\,\frac{\Gamma^*_{\mathbf{k}}}{|\Gamma_{\mathbf{k}}|}. \tag{41}$$

We plot the OAM versus $\mathbf{k}$ for the upper and lower magnon bands in the top and lower panels, respectively, of Fig. 3. The OAM for the two bands are identical for the degenerate bands when $d = 0$ but they differ for the non-degenerate bands when $d > 0$. As seen for the upper or lower bands with $d = 0$, the OAM peaks at the boundaries of the repeated first BZ of the honeycomb lattice. While the OAM of the panels with $d = 0$ obey odd symmetry $O_n(-\mathbf{k}) = -O_n(\mathbf{k})$, the OAM of the panels with $d > 0$ violate this symmetry. The first BZ of the magnetic unit cell is the solid hexagon drawn on the bottom left panel of Fig. 3.

Surprisingly, the results of Fig. 3 are very different than those presented in Refs. [33] and [34], where the linear terms k_α in the OAM operator $\hat{l}_{z\mathbf{k}}$ of Eq. (7) were replaced by periodic functions $\bar{k}_\alpha$,

$$\bar{k}_x a = \sin(3k_x a/2)\cos(\sqrt{3}k_y a/2), \tag{42}$$

$$\bar{k}_y a = \frac{1}{\sqrt{3}}\Big\{\sin(\sqrt{3}k_y a/2)\cos(3k_x a/2) + \sin(\sqrt{3}k_y a)\Big\}, \tag{43}$$

constructed so that $\bar{k}_\alpha(\mathbf{k} + \mathbf{G}_m) = \bar{k}_\alpha(\mathbf{k})$ for any reciprocal lattice vector $\mathbf{G}_m$ of the honeycomb lattice. With

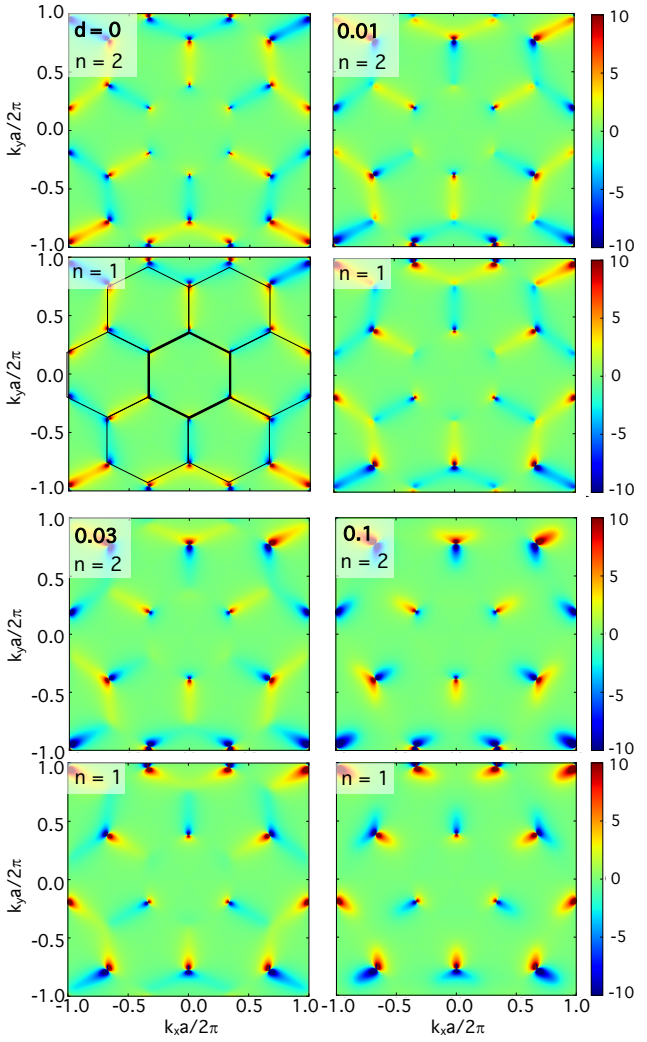

FIG. 3. A honeycomb lattice with FM exchange $J > 0$ between neighboring up spins and DM interaction D between next-nearest neighbors as shown in Fig. 1(c). The OAM $O_n(\mathbf{k})/\hbar$ for the upper, $n = 2$ (top) and lower, $n = 1$ (bottom) bands versus $\mathbf{k}$ for different values of $d = -2D/3J$. The repeated first BZ boundary of the magnetic unit cell (thick solid hexagon) is sketched on the bottom panel for $d = 0$.

the periodic OAM operator

$$\hat{\bar{l}}_{z\mathbf{k}} = -i\left(\bar{k}_x\frac{\partial}{\partial k_y} - \bar{k}_y\frac{\partial}{\partial k_x}\right), \tag{44}$$

the OAM $\overline{O}_n(\mathbf{k})$ also becomes a periodic function of $\mathbf{k}$. By contrast, the OAM plotted in Fig. 3 is clearly not a periodic function. In particular, the OAM $O_n(\mathbf{k})$ increases in size with the magnitude of k. With the periodic $\bar{k}_x$ and $\bar{k}_y$ defined above, Eq. (24) no longer holds and a gauge-invariant, angular-averaged OAM cannot be derived.

For magnon band 1, the gauge-invariant quantity $F_1(k)$ is plotted in Fig. 4(a). For band 2, $F_2(k) = -F_1(k)$, as seen from Fig. 3. With increasing k, $F_1(k)$ oscillates

between positive and negative values and is marked by sharp kinks at its maxima and minima. The positions k for the maxima in $|F_n(k)|$ in Fig. 4(a) correspond to the corners of the hexagons in the lower left panel of Fig. 3, where red and blue regions meet. Notice that $dF_1(k)/dk \geq 0$ while $dF_2(k)/dk \leq 0$ with peaks in the derivatives $|dF_n(k)/dk|$ at the discontinuities of $F_n(k)$.

We emphasize that the OAM must change for different choices of the complex phases $\lambda_n(\mathbf{k})$ in Eqs. (37) and (38). Hence, $O_n(\mathbf{k})$ plotted in Fig. 3 are not themselves observable. However, by integrating $\mathbf{k} = (k, \phi)$ over all angles ϕ for a fixed k, we have resolved that phase ambiguity and created gauge-invariant, observable functions $F_n(k)$.

The functions $O_{1,\mathrm{av}}(k)$ are plotted in Fig. 4(b) for four values of d from 0.001 to 0.1. We find that $O_{1,\mathrm{av}}(k)$ is an oscillatory function that contains cusps at positive peaks when $F_n(k)$ discontinuously drops and negative valleys when $F_n(k)$ rises through 0. The first such cusp lies at the corners of the first hexagonal BZ with $k = 2\sqrt{3}/9(2\pi/a) \approx 0.385(2\pi/a)$. For $d = 0.1$, the average OAM peaks at $0.236\hbar$ at that cusp. Other cusps lie at the corners of the hexagons drawn in the lower left panel of Fig. 3. As k increases, the average OAM tends to zero. By contrast, the average OAM $O_{n,\mathrm{av}}(k)$ of each band of the honeycomb lattice with imposed wavevector periodicity [33] is nonzero (and opposite) as $k \to \infty$. Note that $O_{2,\mathrm{av}}(k) = -O_{1,\mathrm{av}}(k)$ so that the net average of the two bands vanishes.

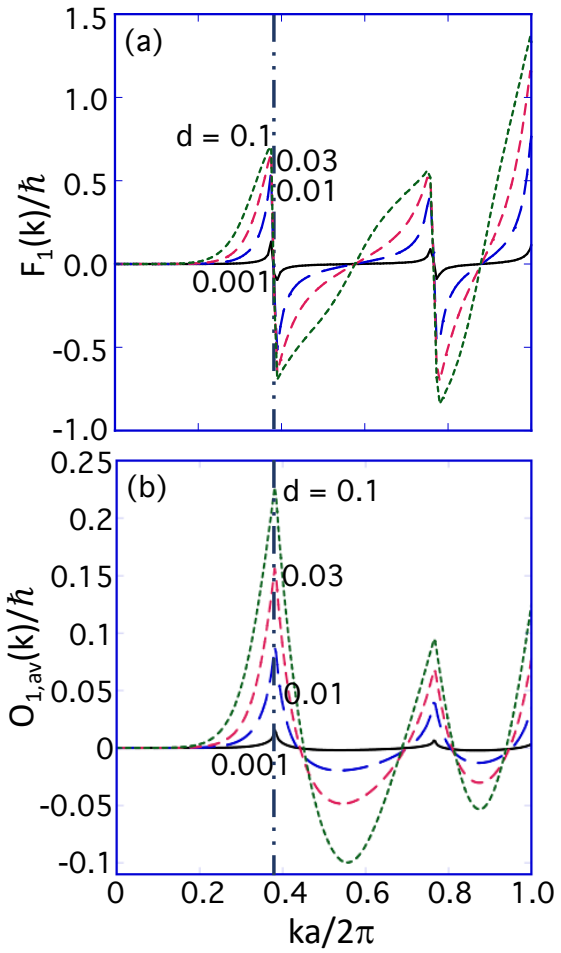

FIG. 4. (a) Gauge-invariant function $F_1(k)/\hbar$ for magnon band 1 of a FM open honeycomb lattice versus k for four values of the DM interaction d. (b) The average OAM $O_{1,\mathrm{av}}(k)/\hbar$ versus $ka/2\pi$ of band 1 for the same four values of d. For magnon band 2, $F_2(k) = -F_1(k)$ and $O_{2,\mathrm{av}}(k) = -O_{1,\mathrm{av}}(k)$. The dot-dash vertical line marks $k_{\max}$ for the first BZ in both (a) and (b).

V. TRANSLATING BETWEEN THE SEMICLASSICAL AND QUANTUM LANGUAGES

In order to reconcile Eqs. (2) and (19) for the Berry phase, we must we must define

$$\langle u_n(\mathbf{k})|\hat{A}|u_n(\mathbf{k})\rangle_{\mathrm{cell}} \equiv \sum_{r=1}^{M} \langle \underline{v}_{rn}(\mathbf{k})|\hat{A}\,\underline{N}|\underline{v}_{rn}(\mathbf{k})\rangle, \quad (45)$$

where

$$|\underline{v}_{rn}(\mathbf{k})\rangle = \begin{pmatrix} X^{-1}_{rn}(\mathbf{k}) \\ X^{-1}_{r+M,n}(\mathbf{k}) \end{pmatrix}, \quad (46)$$

$$\langle \underline{v}_{rn}(\mathbf{k})| = \left(X^{-1}_{rn}(\mathbf{k})^*, X^{-1}_{r+M,n}(\mathbf{k})^* \right), \quad (47)$$

and the integral over the magnetic unit cell on the *lhs* of Eq. (45) is replaced by a sum over sites r within the magnetic unit cell on the *rhs* of that expression. As required, this transformation implies that

$$\begin{aligned} \langle u_n(\mathbf{k})|\hat{I} \quad & |u_n(\mathbf{k})\rangle \\ &= \sum_{r=1}^{M} \langle \underline{v}_{rn}(\mathbf{k})|\underline{N}|\underline{v}_{rn}(\mathbf{k})\rangle \\ &= \sum_{r=1}^{M} \left\{ |X^{-1}(\mathbf{k})_{rn}|^2 - |X^{-1}(\mathbf{k})_{r+M,n}|^2 \right\} \\ &= 1, \end{aligned} \quad (48)$$

which uses the normalization condition of Eq. (23).

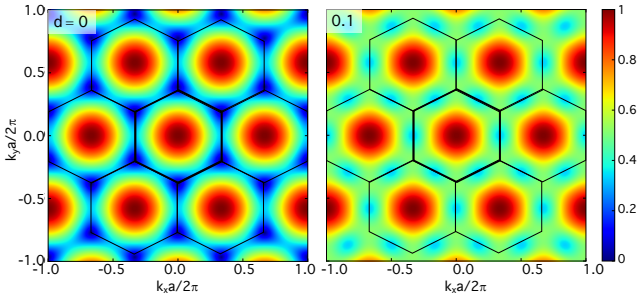

FIG. 5. The splitting $\eta_{\mathbf{k}}$ between magnon bands $n = 1$ and $n = 2$ of the FM open honeycomb lattice with $d = 0$ (left) or 0.1 (right). The first BZ is shown by the solid hexagon in both figures.

VI. DISCUSSION

The function $F_n(k)$ gives the average OAM over a ring with wavevector k. Because it is gauge invariant, $F_n(k)$ is also measureable. It yields the average OAM at $k = |\mathbf{k}|$, but not the angles ϕ at which that OAM can be detected. One of the greatest barriers to studies of the OAM at wavevector $\mathbf{k}$ has been its lack of gauge invariance. By integrating the OAM over the orientation ϕ of $\mathbf{k}$, we have constructed gauge-invariant functions $F_n(k)$ and $O_{n,\mathrm{av}}(k)$ that are nonzero for the FM honeycomb lattice but vanish for the AF honeycomb lattice and in the absence of DM interactions.

While $O_n(\mathbf{k})$ is not a periodic function of $\mathbf{k}$, physical quantities like $\mathcal{L}_z$ in Eq. (16) impose limits on the wavevector $\mathbf{k}$ by summing over the first BZ of the magnetic unit cell. For the FM honeycomb lattice, the magnetic unit cell is the hexagon sketched in the inset to Fig. 3. The maximum amplitude of the wavevector within the first BZ lies at its corners with $k_{\max} = 2\sqrt{3}/9(2\pi/a) \approx 0.385(2\pi)/a$.

It is doubtful that a magnon with wavevector outside the first BZ has any physical significance. Certainly, any such magnon would rapidly decay via higher-order quantum processes into single magnons within the first BZ while conserving energy, momentum, spin, and OAM. Considering only magnons within the first BZ of the open honeycomb lattice, we can reach several conclusions. From Fig. 4, we see that both $F_1(k)$ and $O_{1,\mathrm{av}}(k)$ (band 1) are positive for all k within the first BZ. For $d = 0.1$, band 1 will then have an average OAM of about $0.24\hbar$ while band 2 will have an average OAM of about $-0.24\hbar$.

A natural question is whether angular averages over ϕ make sense for k near $k_{\max}$ if only wavevectors $\mathbf{k}$ within the first BZ are physical since those angular averages must also include wavevectors outside the first BZ. However, the same numerical results are obtained while restricting the integral for $F_n(k)$ to include wavevectors $\mathbf{k}$ solely within the first BZ because the large OAM just inside the BZ corners dominate the integral over ϕ for k near $k_{\max}$.

Experiments can tune the OAM by changing the splitting of the magnon bands with energies $\hbar\omega_{1,2}(\mathbf{k})/3JS = 1 + \kappa \mp \eta_{\mathbf{k}}$ from Eqs. (31) and (32) and

$$\eta_{\mathbf{k}} = \sqrt{|\Gamma_{\mathbf{k}}|^2 + d^2\,\Theta_{\mathbf{k}}^2}. \tag{49}$$

Plotted in Fig. 5, $\eta_{\mathbf{k}}$ has minima of 0 at the sides of the BZ for $d = 0$ or of $1/3$ at the midpoints of the sides for $d = 0.1$; $\eta_{\mathbf{k}}$ has an absolute maximum of 1 independent of d at $\mathbf{k} = 0$ and a relative maximum of $3\sqrt{3}\,d \approx 0.51$ for $d = 0.1$ at the corners of the BZ, where $\Gamma_{\mathbf{k}} = 0$. Therefore, searches for OAM in FM honeycomb materials with significant DM interactions should concentrate at wavevectors with amplitude $k = 0.385(2\pi)/a$, where the splitting between magnon bands is approximately $18\sqrt{3}\,dJS = 12\sqrt{3}|D|S$, independent of the exchange J. Note that the splitting between the upper and lower magnon bands is due to the broken time-reversal symmetry produced by the DM interaction.

If a high-energy electron beam [29] with transverse momentum $ka/2\pi \approx 0.38$ and OAM $L_z = -\hbar$ strikes a FM honeycomb sample (like CrI_3 [43, 44] or $CrCl_3$ [45]) with $d \approx 0.1$, then Fig. 4(a) predicts that it is likely to encounter a magnon with $ka/2\pi \approx 0.38$ and opposite OAM $L_z = \hbar$. But the wavevector orientation ϕ of that magnon is not determined. Keep in mind, though, that that the function $F_n(k)$ must be averaged over the radial spread Δk of the magnon wavepacket [40].

Several important questions remain unanswered. Precisely how can $F_n(k)$ be measured? In what other systems would $F_n(k)$ be nonzero? How do the magnon orbital and spin angular momentum couple to one another? We are hopeful that future work will provide answers to these questions as the field of magnonic OAM attracts renewed interest.

Satoshi Okamoto and Giovanni Vignale helped this work with useful conversations. Research sponsored by the U.S. Department of Energy, Office of Science, Basic Energy Sciences, Materials Sciences and Engineering Division. The data that support the findings of this study are available from the author upon reasonable request.

[1] O. Bttner, M. Bauer, A. Rueff, S.O. Demokritov, B. Hillebrands, A.N. Slavin, M.P. Kostylev, and B.A. Kalinikos. Space- and time-resolved Brillouin light scattering from nonlinear spin-wave packets. *Ultrasonics* **38**, 443 (2000).

[2] Max Hirschberger, Jason W. Krizan, R. J. Cava, and

N. P. Ong. Large thermal Hall conductivity of neutral spin excitations in a frustrated quantum magnet. *Science* **348**, 106 (2015).

[3] Max Hirschberger, Robin Chisnell, Young S. Lee, and N. P. Ong. Thermal Hall effect of spin excitations in a Kagome magnet. *Phys. Rev. Lett.* **115**, 106603 (2015).

[4] Shuichi Murakami and Akihiro Okamoto. Thermal Hall effect of magnons. *Journal of the Physical Society of Japan* **86**, 011010 (2017).

[5] Robin R. Neumann, Alexander Mook, Jürgen Henk, and Ingrid Mertig. Thermal Hall effect of magnons in collinear antiferromagnetic insulators: Signatures of magnetic and topological phase transitions. *Phys. Rev. Lett.* **128**, 117201 (2022).

[6] Ken-ichi Uchida, Hiroto Adachi, Takeru Ota, Hiroyasu Nakayama, Sadamichi Maekawa, and Eiji Saitoh. Observation of longitudinal spin-Seebeck effect in magnetic insulators. *Applied Physics Letters* **97**, 172505 (2010).

[7] Stephen M. Wu, Wei Zhang, Amit KC, Pavel Borisov, John E. Pearson, J. Samuel Jiang, David Lederman, Axel Hoffmann, and Anand Bhattacharya. Antiferromagnetic spin Seebeck effect. *Phys. Rev. Lett.* **116**, 097204 (2016).

[8] Ran Cheng, Satoshi Okamoto, and Di Xiao. Spin Nernst effect of magnons in collinear antiferromagnets. *Phys. Rev. Lett.* **117**, 217202 (2016).

[9] Vladimir A. Zyuzin and Alexey A. Kovalev. Magnon spin Nernst effect in antiferromagnets. *Phys. Rev. Lett.* **117**, 217203 (2016).

[10] Hantao Zhang and Ran Cheng. A perspective on magnon spin Nernst effect in antiferromagnets. *Applied Physics Letters* **120**, 090502 (2022).

[11] X. S. Wang and X. R. Wang. Topological magnonics. *Journal of Applied Physics* **129**, 151101 (2021).

[12] A. V. Chumak, P. Kabos, M. Wu, C. Abert, C. Adelmann, A. O. Adeyeye, J. kerman, F. G. Aliev, A. Anane, A. Awad, C. H. Back, A. Barman, G. E. W. Bauer, M. Becherer, E. N. Beginin, V. A. S. V. Bittencourt, Y. M. Blanter, P. Bortolotti, I. Boventer, D. A. Bozhko, S. A. Bunyaev, J. J. Carmiggelt, R. R. Cheenikundil, F. Ciubotaru, S. Cotofana, G. Csaba, O. V. Dobrovolskiy, C. Dubs, M. Elyasi, K. G. Fripp, H. Fulara, I. A. Golovchanskiy, C. Gonzalez-Ballestero, P. Graczyk, D. Grundler, P. Gruszecki, G. Gubbiotti, K. Guslienko, A. Haldar, S. Hamdioui, R. Hertel, B. Hillebrands, T. Hioki, A. Houshang, C.-M. Hu, H. Huebl, M. Huth, E. Iacocca, M. B. Jungfleisch, G. N. Kakazei, A. Khitun, R. Khymyn, T. Kikkawa, M. Klui, O. Klein, J. W. Kos, S. Knauer, S. Koraltan, M. Kostylev, M. Krawczyk, I. N. Krivorotov, V. V. Kruglyak, D. Lachance-Quirion, S. Ladak, R. Lebrun, Y. Li, M. Lindner, R. Macdo, S. Mayr, G. A. Melkov, S. Mieszczak, Y. Nakamura, H. T. Nembach, A. A. Nikitin, S. A. Nikitov, V. Novosad, J. A. Otlora, Y. Otani, A. Papp, B. Pigeau, P. Pirro, W. Porod, F. Porrati, H. Qin, B. Rana, T. Reimann, F. Riente, O. Romero-Isart, A. Ross, A. V. Sadovnikov, A. R. Safin, E. Saitoh, G. Schmidt, H. Schultheiss, K. Schultheiss, A. A. Serga, S. Sharma, J. M. Shaw, D. Suess, O. Surzhenko, K. Szulc, T. Taniguchi, M. Urbnek, K. Usami, A. B. Ustinov, T. van der Sar, S. van Dijken, V. I. Vasyuchka, R. Verba, S. Viola Kusminskiy, Q. Wang, M. Weides, M. Weiler, S. Wintz, S. P. Wolski, and X. Zhang. Advances in magnetics roadmap on spin-wave computing. *IEEE Transactions on Magnetics* **58**, 1 (2022).

[13] Denis D. Sheka, Oleksandr V. Pylypovskyi, Oleksii M. Volkov, Kostiantyn V. Yershov, Volodymyr P. Kravchuk, and Denys Makarov. Fundamentals of curvilinear ferromagnetism: Statics and dynamics of geometrically curved wires and narrow ribbons. *Small* **18**, 2105219 (2022).

[14] J. E. Hirsch. Spin Hall effect. *Phys. Rev. Lett.* **83**, 1834 (1999).

[15] Shufeng Zhang. Spin Hall effect in the presence of spin diffusion. *Phys. Rev. Lett.* **85**, 393 (2000).

[16] Y. Onose, T. Ideue, H. Katsura, Y. Shiomi, N. Nagaosa, and Y. Tokura. Observation of the magnon Hall effect. *Science* **329**, 297 (2010).

[17] Hosho Katsura, Naoto Nagaosa, and Patrick A. Lee. Theory of the thermal Hall effect in quantum magnets. *Phys. Rev. Lett.* **104**, 066403 (2010).

[18] Di Xiao, Ming-Che Chang, and Qian Niu. Berry phase effects on electronic properties. *Rev. Mod. Phys.* **82**, 1959 (2010).

[19] Akihiro Okamoto and Shuichi Murakami. Berry curvature for magnons in ferromagnetic films with dipole-exchange interactions. *Phys. Rev. B* **96**, 174437 (2017).

[20] Ryo Matsumoto and Shuichi Murakami. Theoretical prediction of a rotating magnon wave packet in ferromagnets. *Phys. Rev. Lett.* **106**, 197202 (2011).

[21] Ryo Matsumoto and Shuichi Murakami. Rotational motion of magnons and the thermal Hall effect. *Phys. Rev. B* **84**, 184406 (2011).

[22] Yijie Shen, Xuejiao Wang, Zhenwei Xie, Changjun Min, Xing Fu, Qiang Liu, Mali Gong, and Xiaocong Yuan. Optical vortices 30 years on: OAM manipulation from topological charge to multiple singularities. *Light: Science & Applications* **8**, 90 (2019).

[23] Yiqi Fang, Shengyue Lu, and Yunquan Liu. Controlling photon transverse orbital angular momentum in high harmonic generation. *Phys. Rev. Lett.* **127**, 27 (2021).

[24] Guillermo F. Quinteiro Rosen, Pablo I. Tamborenea, and Tilmann Kuhn. Interplay between optical vortices and condensed matter. *Rev. Mod. Phys.* **94**, 3 (2022).

[25] Jonas Wätzel, Primo ž Rebernik Ribič, Marcello Coreno, Miltcho B. Danailov, Christian David, Alexander Demidovich, Michele Di Fraia, Luca Giannessi, Klavs Hansen, Špela Krušič, Michele Manfredda, Michael Meyer, Andrej Mihelič, Najmeh Mirian, Oksana Plekan, Barbara Ressel, Benedikt Rösner, Alberto Simoncig, Simone Spampinati, Matija Stupar, Matja ž Žitnik, Marco Zangrando, Carlo Callegari, Jamal Berakdar, and Giovanni De Ninno. Light-induced magnetization at the nanoscale. *Phys. Rev. Lett.* **128**, 157205 (2022).

[26] Dongwook Go, Daegeun Jo, Hyun-Woo Lee, Mathias Klui, and Yuriy Mokrousov. Orbitronics: Orbital currents in solids. *EPL (Europhysics Letters)* **135**, 37001 (2021).

[27] Seungyun Han, Hyun-Woo Lee, and Kyoung-Whan Kim. Orbital dynamics in centrosymmetric systems. *Phys. Rev. Lett.* **128**, 176601 (2022).

[28] Oliver Dowinton and Mohammad Saeed Bahramy. Orbital angular momentum driven anomalous Hall effect. *Phys. Rev. B* **105**, 235142 (2022).

[29] B.G. Mendis. Quantum theory of magnon excitation by high energy electron beams. *Ultramicroscopy* **239**, 113548 (2022).

[30] Lifa Zhang and Qian Niu. Angular momentum of phonons and the Einstein–de Haas effect. *Phys. Rev.*

Lett. **112**, 085503 (2014).

[31] Masato Hamada, Emi Minamitani, Motoaki Hirayama, and Shuichi Murakami. Phonon angular momentum induced by the temperature gradient. *Phys. Rev. Lett.* **121**, 175301 (2018).

[32] L. Marrucci, C. Manzo, and D. Paparo. Optical spin-to-orbital angular momentum conversion in inhomogeneous anisotropic media. *Phys. Rev. Lett.* **96**,163905 (2006).

[33] Randy S. Fishman, Jason S. Gardner, and Satoshi Okamoto. Orbital angular momentum of magnons in collinear magnets. *Phys. Rev. Lett.* **129**, 167202 (2022).

[34] Randy S. Fishman, Lucas Lindsay, and Satoshi Okamoto. Exact results for the orbital angular momentum of magnons on honeycomb lattices. *Journal of Physics: Condensed Matter* **35**, 015801 (2022).

[35] Takahiro Fukui, Yasuhiro Hatsugai, and Hiroshi Suzuki. Chern numbers in discretized Brillouin zone: Efficient method of computing (spin) Hall conductances. *Journal of the Physical Society of Japan* **74**, 1674 (2005).

[36] V. M. Tsukernik. Some Features of the Gyromagnetic Effect in Ferrodielectrics at Low Temperatures. *Soviet Journal of Experimental and Theoretical Physics* **50**, 1631 (1966).

[37] V. S. Garmatyuk and V. M. Tsukernik. The Gyromagnetic Effect in an Antiferromagnet at Low Temperatures. *Soviet Journal of Experimental and Theoretical Physics* **26**, 1035 (1968).

[38] L.D. Landau and E.M. Lifshitz. *The Classical Theory of Fields*. (Butterworth-Heinemann, Fourth revised English edition, 1973).

[39] Randy S. Fishman, Jaime Fernandez-Baca, and Toomas Rõõm. *Spin-Wave Theory and its Applications to Neutron Scattering and THz Spectroscopy*. (Morgan and Claypool Publishers, San Rafael, 2018).

[40] Ming-Che Chang and Qian Niu. Berry phase, hyperorbits, and the Hofstadter spectrum: Semiclassical dynamics in magnetic Bloch bands. *Phys. Rev. B* **53**, 7010 (1996).

[41] Randy S. Fishman, Jason S. Gardner, and Satoshi Okamoto. Erratum: Orbital angular momentum of magnons in collinear magnets [Phys. Rev. Lett. **129**, 167202 (2022)]. *Phys. Rev. Lett.* **130**, 059901 (2023).

[42] The integral over ϕ is *not* a line integral over a closed loop such as enters the Chern number:

$$p_n = \oint_C d\mathbf{k} \cdot \mathbf{A}_n(\mathbf{k}) = \int_S d\mathbf{S} \cdot \mathbf{\Omega}_n(\mathbf{k}), \tag{50}$$

which uses Stokes theorem with $\mathbf{\Omega}_n = \partial/\partial\mathbf{k} \times \mathbf{A}_n$ and

$$\mathbf{A}_n(\mathbf{k}) = \frac{i}{2\pi}\langle u_n(\mathbf{k})|\frac{\partial}{\partial\mathbf{k}}|u_n(\mathbf{k})\rangle. \tag{51}$$

The *lhs* of Eq. (50) can then take any multiple of 2π [11]. By contrast, the integrals over ϕ in Eqs. (25) and (26) are proper Riemann integrals from 0 to 2π where $\mathbf{k}_0 = (k, 0) = (k, 2\pi)$.

[43] Michael A. McGuire, Hemant Dixit, Valentino R. Cooper, and Brian C. Sales. Coupling of crystal structure and magnetism in the layered, ferromagnetic insulator CrI_3. *Chemistry of Materials* **27**, (2015).

[44] Lebing Chen, Jae-Ho Chung, Bin Gao, Tong Chen, Matthew B. Stone, Alexander I. Kolesnikov, Qingzhen Huang, and Pengcheng Dai. Topological spin excitations in honeycomb ferromagnet CrI_3. *Phys. Rev. X* **8**, 041028, (2018).

[45] Xun Li, Seung-Hwan Do, Jiaqiang Yan, Michael A. McGuire, Garrett E. Granroth, Sai Mu, Tom Berlijn, Valentino R. Cooper, Andrew D. Christianson, and Lucas Lindsay. Phonons and phase symmetries in bulk $CrCl_3$ from scattering measurements and theory. *Acta Materialia* **241**, 118390 (2022).